



## OPEN ACCESS

## EDITED BY

Wei-Chih Lai,  
National Cheng Kung University, Taiwan

## REVIEWED BY

Chih Wei Chu,  
Academia Sinica, Taiwan  
Boping Yang,  
Hubei University of Automotive  
Technology, China

## \*CORRESPONDENCE

Lung-Chien Chen,  
✉ ocean@ntut.edu.tw

RECEIVED 13 January 2025

ACCEPTED 25 April 2025

PUBLISHED 20 May 2025

## CITATION

Weng W-S, Chien Y-C, Lee T-Y and Chen L-C  
(2025) Study of MASnI<sub>3</sub> perovskite  
photodetectors prepared by the inverse  
temperature crystallization method in  
ambient atmosphere and the spin coating  
method in a glovebox.  
*Front. Mater.* 12:1559686.  
doi: 10.3389/fmats.2025.1559686

## COPYRIGHT

© 2025 Weng, Chien, Lee and Chen. This is an  
open-access article distributed under the  
terms of the [Creative Commons Attribution  
License \(CC BY\)](#). The use, distribution or  
reproduction in other forums is permitted,  
provided the original author(s) and the  
copyright owner(s) are credited and that the  
original publication in this journal is cited, in  
accordance with accepted academic practice.  
No use, distribution or reproduction is  
permitted which does not comply with  
these terms.

# Study of MASnI<sub>3</sub> perovskite photodetectors prepared by the inverse temperature crystallization method in ambient atmosphere and the spin coating method in a glovebox

Wei-Sung Weng<sup>1</sup>, Yu-Ching Chien<sup>2</sup>, Tsung-Yen Lee<sup>3</sup> and Lung-Chien Chen<sup>2\*</sup>

<sup>1</sup>Department of Avionics, China University of Science and Technology, Taipei, Taiwan, <sup>2</sup>Department of Electro-Optical Engineering, National Taipei University of Technology, Taipei, Taiwan, <sup>3</sup>Department of Mechanical Engineering, National Taipei University of Technology, Taipei, Taiwan

In this study, we prepared MASnI<sub>3</sub> lead (Pb)-free halide perovskite metal-semiconductor-metal-type photodetectors through the inversion crystallization method under an atmospheric environment and the spin-coating method in a glove box, respectively. The scanning electron microscopy (SEM) images revealed the different surface morphology. They show two types of growth models: the inverse temperature crystallization (ITC) method uses solvent volatilization, and the spin-coating method is a reaction between precursors. For the MASnI<sub>3</sub> perovskite film obtained through the inversion crystallization method, a broad band of photoluminescence (PL) spectrum at approximately 470 nm, corresponding to the level transition of 2.638 eV, was observed. On the other hand, for the MASnI<sub>3</sub> perovskite film obtained through the spin-coating method, a narrow band of the photoluminescence spectrum at approximately 773 nm, corresponding to the level transition of 1.604 eV, was observed. This is the Burstein–Moss shift environment due to the introduction of oxygen. In addition, the photocurrent of a device prepared in a glove box is two orders of magnitude higher than that of the device prepared by the ITC method.

## KEYWORDS

perovskite, MASnI<sub>3</sub>, photodetectors, Burstein–Moss shift, oxidation

## 1 Introduction

In the early part of this decade, the halide perovskite materials, like MAPbBr<sub>3</sub>, were mostly lead (Pb)-containing halide perovskites. Except for the outstanding optoelectronic properties, including high charge carrier mobility, defect tolerance, and high absorption, the characteristics regarding pinhole formation and crystallinity of perovskite materials are suitable for the application of gas sensors (Kassa et al., 2025; Lee et al., 2025; Zhai et al., 2024). However, lead-containing materials in many other related products have been proven to gradually decompose over time, making it easy to be exposed to excessive lead during use. In subsequent research on halide perovskites, it was confirmed that the lead

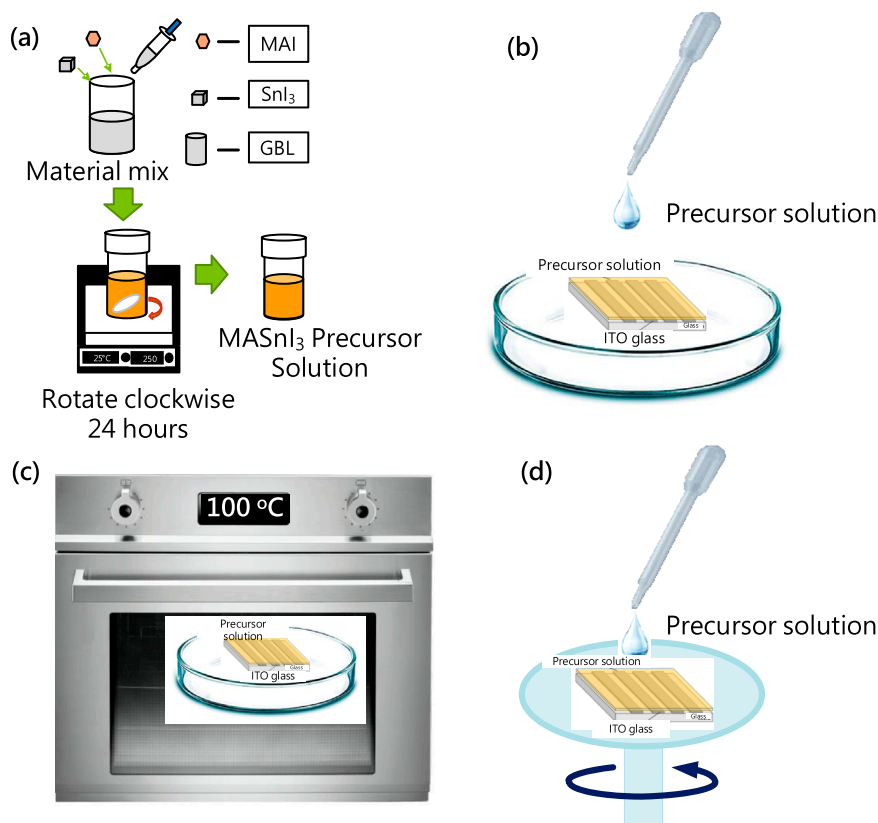


**FIGURE 1** Process of lead-free MASnI<sub>3</sub> perovskite metal-semiconductor-metal type photodetector: (a) precursor preparation, (b) precursor coating and (c) baking, and (d) precursor spin coating.

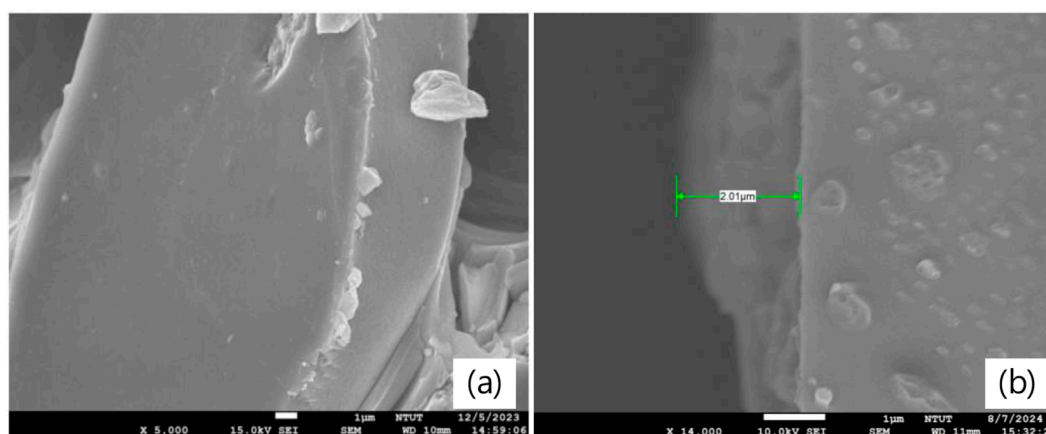


**FIGURE 2** Cross-sectional SEM image of MASnI<sub>3</sub> perovskite films prepared by (a) ITC and (b) spin coating, respectively.

in halide perovskites is easily soluble in water after oxidation over time, thereby polluting the environment (Wan et al., 2021). This has played an important role in promoting the research and development of lead-free halide perovskites. Among them, both tin (Sn) and lead belong to the same group of elements and have similar chemical properties, and their close covalent radii have

a greater impact on the structural stability of halide perovskites. MASnI<sub>3</sub> is an interesting material due to its very easy oxidation and degradation in ambient air. Therefore, only a few studies have compared Pb-based perovskite materials and MASnI<sub>3</sub>. The pollution caused by oxides is much less harmful than lead, making tin a popular choice to replace lead as lead-free halide perovskites,

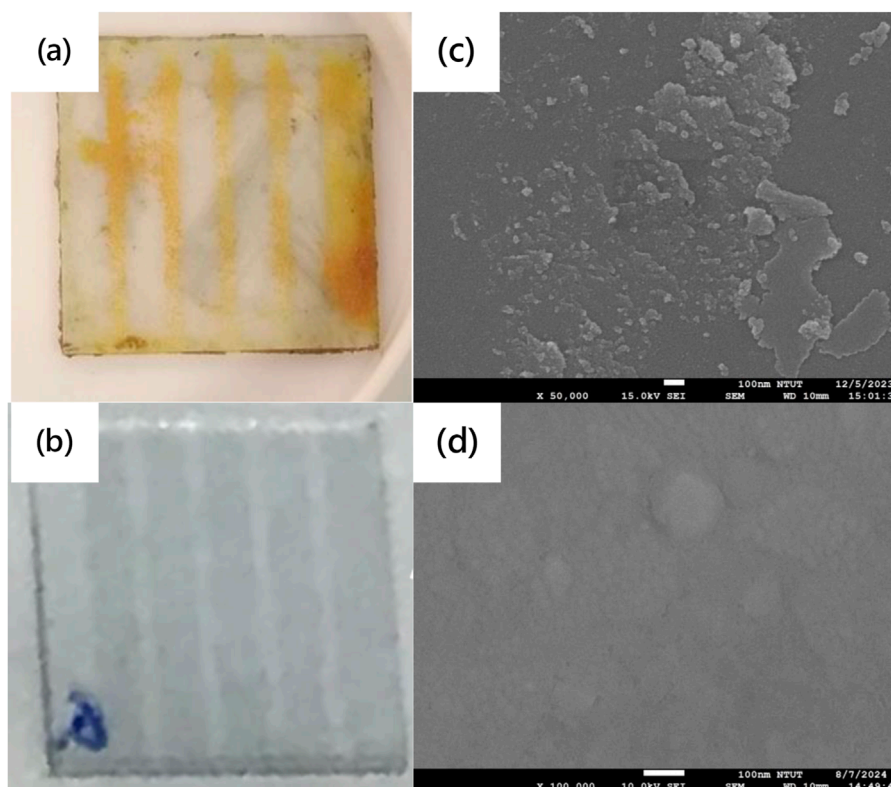


**FIGURE 3** (a,b) Photo and (c,d) top-view SEM image of  $\text{MASnI}_3$  perovskite metal-semiconductor-metal-type photodetectors prepared in air and in a glove box, respectively.

and has generated a large amount of related research (Hao et al., 2015; Noel et al., 2014; Hao et al., 2014; Stoumpos et al., 2013; Chen et al., 2016). However, tin in  $\text{ABX}_3$  halide perovskite easily transforms from  $\text{Sn}^{2+}$  to  $\text{Sn}^{4+}$ , thereby destroying the stability of the structure of perovskite materials (Mitzi and Liang, 1997; Sabba et al., 2015; Yuan et al., 2022; Peng and Xie, 2020; Bouich et al., 2022; Aldamasy et al., 2021; Saha et al., 2024). Therefore, a key problem that must be solved is that these devices must overcome the degradation in the ambient environment to be profitable. This study used the halide perovskite  $\text{MASnI}_3$  as a photodetector material. In this work, we carried out the device process by the inverse temperature crystallization (ITC) method under a normal atmospheric environment to make an  $\text{MASnI}_3$  halide perovskite film on the glass substrates with an ITO electrode pattern and observed their surface images with SEM. The image of the film growth crystal and the I-V characteristics were investigated using a photocurrent induced by different wavelengths of visible light and infrared. In addition, we prepared the  $\text{MASnI}_3$  perovskite film deposited by the spin-coating method to compare the different characteristics of films obtained by the ITC and spin coating methods.

## 2 Materials and methods

First, the MAI (0.11 g) and  $\text{SnI}_2$  (0.27 g), respectively, were put in a glass beaker, and then a pipette was used to add 0.5 mL of

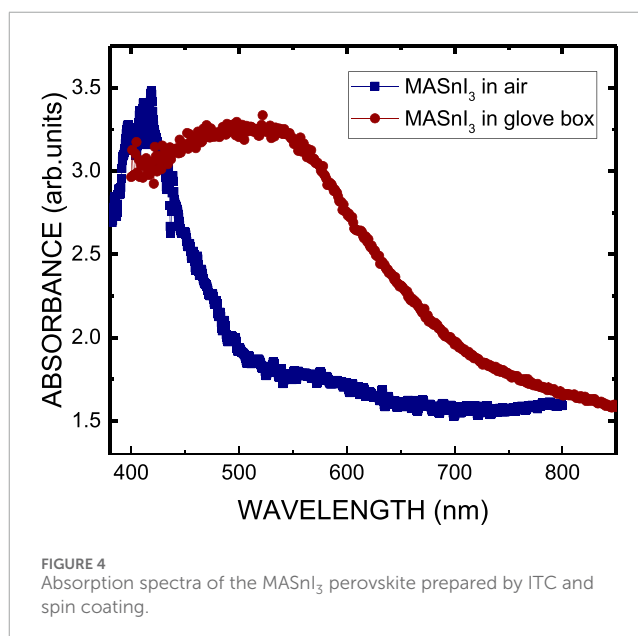


**FIGURE 4** Absorption spectra of the  $\text{MASnI}_3$  perovskite prepared by ITC and spin coating.

$\gamma$ -butyrolactone (GBL) solution into the glass beaker, which was stirred with a magnet that was cleaned using ethanol and blown dry with nitrogen. The beaker was sealed with tape and placed on an electromagnetic heating stirrer to stir at 500 rpm for 24 h to form a

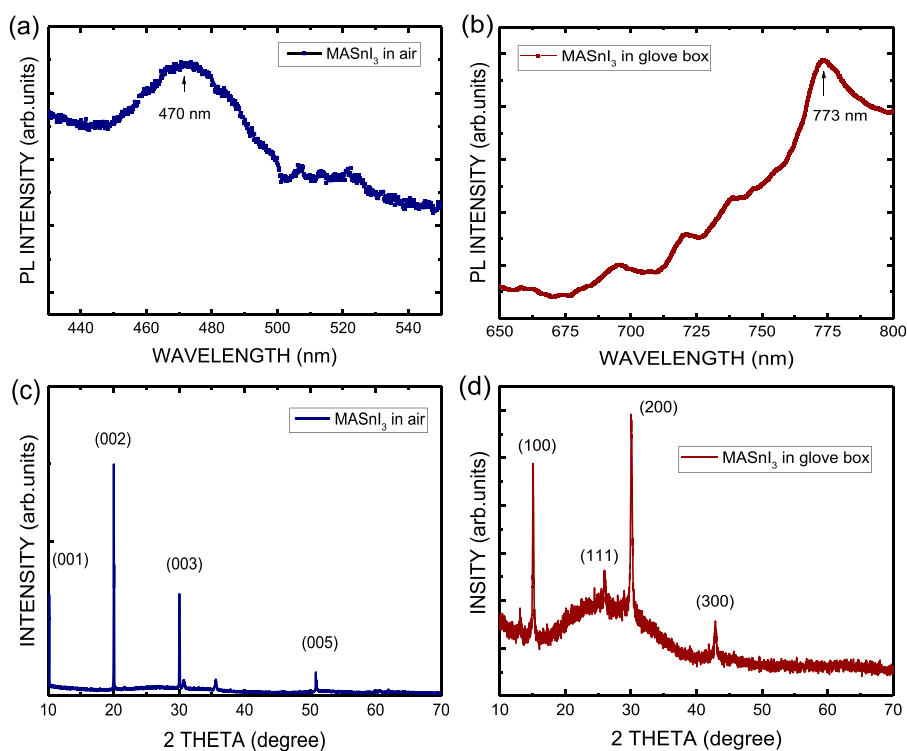


FIGURE 5

Photoluminescence (PL) spectra of the  $\text{MASnI}_3$  perovskite prepared by (a) ITC and (b) spin coating. XRD patterns of the  $\text{MASnI}_3$  perovskite prepared by (c) ITC and (d) spin coating, respectively.

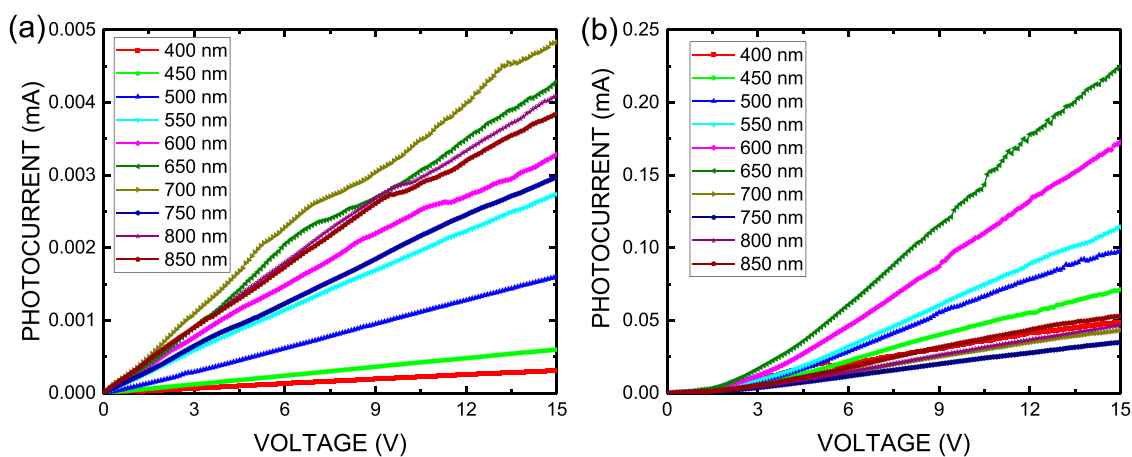


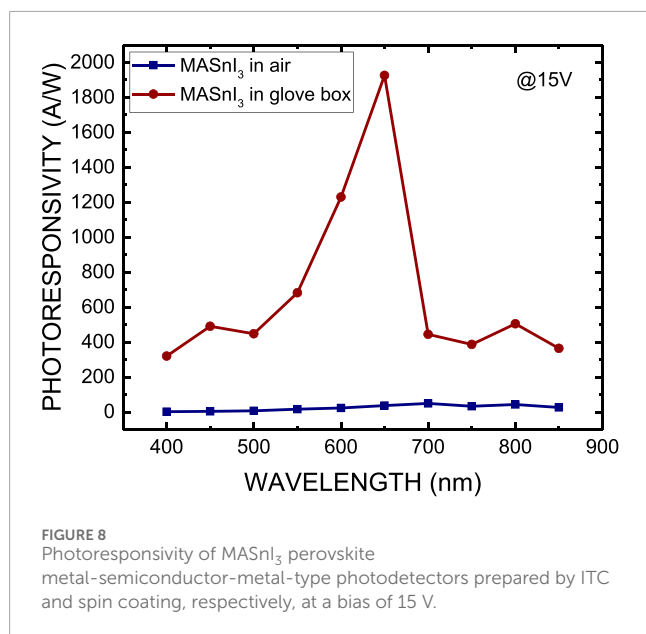
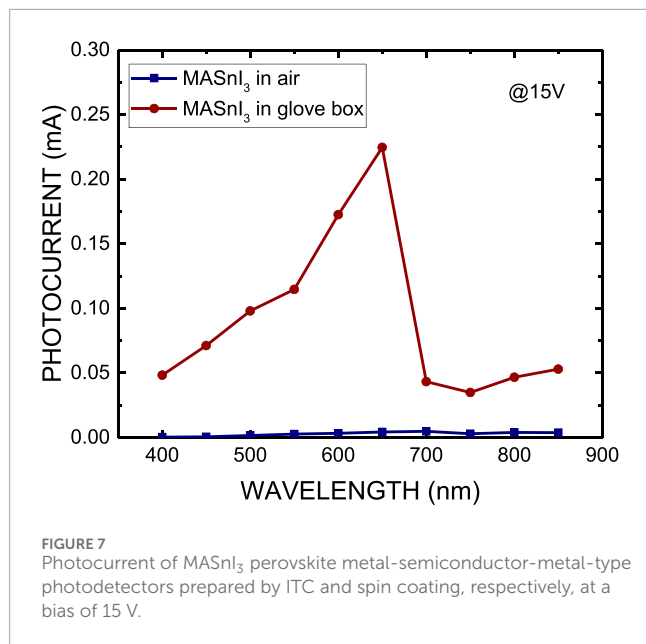
FIGURE 6

(a) Current–voltage ( $I$ – $V$ ) characteristics and (b) responsivity of  $\text{MASnI}_3$  perovskite metal–semiconductor–metal–type photodetectors.

1.5 M  $\text{MASnI}_3$  precursor solution, as shown in Figure 1a (Yuan et al., 2022; Peng and Xie, 2020). Next, the ITO glass was cleaned with an ultrasonic oscillator using organic acetone or IPA solution for 5 min. It was placed in an ultraviolet lighting machine for 10 min to form a hydrophilic surface. Then, the  $\text{MASnI}_3$  precursor solution was dropped onto the surface of the ITO glass substrate and moved into an oven for baking at  $100^\circ\text{C}$  for approximately 5–7 days to form the  $\text{MASnI}_3$  film, as shown in Figures 1b,c. For the second sample, we

prepared the  $\text{MASnI}_3$  perovskite film metal–semiconductor–metal–type photodetector on the glass substrate with an ITO pattern deposited by the spin-coating method (3,000 rpm) using the same precursor solution, as shown in Figure 1d.

The crystallinities of  $\text{MASnI}_3$  perovskite on glass substrates with ITO electrodes were examined by an X-ray diffractometer (Almelo, Netherlands) with a Cu-target ( $\lambda = 1.5418 \text{ \AA}$ ) source. The photoluminescence (PL) spectra and electronic properties of the



photodetectors were obtained using a current source meter and spectrophotometer. The photocurrents of devices are obtained by an F-7000 fluorescence spectrophotometer with a 150-W xenon lamp.

### 3 Results and discussion

Figures 2a,b show the cross-sectional SEM image of MASnI<sub>3</sub> perovskite films prepared by the ITC and spin-coating methods to check their thicknesses, respectively. The thicknesses of MASnI<sub>3</sub> perovskite films prepared by the ITC and spin-coating methods are 20  $\mu\text{m}$  and 2  $\mu\text{m}$ , respectively. Figures 3a,b show the picture and top-view SEM images of MASnI<sub>3</sub> perovskite metal-semiconductor-metal type photodetectors. A 20- $\mu\text{m}$ -thick MASnI<sub>3</sub> perovskite film

with yellow color was formed on the glass substrate with an ITO electrode pattern by the inverse temperature crystallization (ITC) method. Under the observation of the top-view SEM image, as shown in Figure 3b, the morphology of the MASnI<sub>3</sub> thin film at  $\times 50,000$  magnification shows a relatively flat pattern, but there are some flow lines and particles on the surface. The flow lines may have contributed to the MASnI<sub>3</sub> perovskite precursor solution drying in the oven when the MASnI<sub>3</sub> perovskite film was growing. The particles are the substances produced by the oxidation of MASnI<sub>3</sub> perovskite material. In contrast, the MASnI<sub>3</sub> perovskite film grown in a glove box shows a gray color, as shown in Figure 3c. It is a typical color for the MASnI<sub>3</sub> perovskite film. The morphology of the MASnI<sub>3</sub> perovskite film grown in a glove box is quite smooth with several small hills on the surface, as shown in Figure 3d. There are two types of growth models: the former is solvent volatilization, and the latter is a reaction between precursors. The solvent volatilization naturally results in precursor oversaturation and nucleation deposition. The surface with a small hill prepared by the spin-coating method is Stransky–Krastanov (SK) growth caused by the deposition of MASnI<sub>3</sub> perovskite thin film, owing to the solvent volatilizing quickly.

Figure 4 shows the absorption spectra of MASnI<sub>3</sub> perovskite on glass substrate prepared by the ITC method in air and spin coating in a glove box, respectively. Their optical absorption edges are 490 nm and 770 nm, respectively. Figure 5a shows the photoluminescence (PL) spectra of the MASnI<sub>3</sub> perovskite on a glass substrate prepared by the ITC method in air. The peak position of the PL spectrum is approximately 470 nm, corresponding to the level transition of 2.638 eV. The band gap of MASnI<sub>3</sub> perovskite is 1.604 eV, theoretically (Bouich et al., 2022). As shown in Figure 5b, the location of the PL peak of the MASnI<sub>3</sub> perovskite film grown by spin coating in a glove box is 773 nm. It corresponds to the theoretical position. The broad PL spectrum of MASnI<sub>3</sub> may contribute to the effect of the Burstein–Moss shift caused by the oxidation of MASnI<sub>3</sub> because the material was prepared under an ambient atmosphere (Chen et al., 2006; Walukiewicz et al., 2004). Figure 5c plots the X-ray diffraction (XRD) pattern of the MASnI<sub>3</sub> perovskite on glass substrate and shows a P-3m1 phase and a narrow full width at half maximum (FWHM) of the diffraction peak. Four main peaks appear at the diffracted peak positions  $2\theta = 10.2^\circ$ ,  $19.7^\circ$ ,  $30.0^\circ$ , and  $50.9^\circ$ , corresponding to the crystal planes (001), (002), (003), and (005), respectively. It confirmed the formation of a single crystal of MASnI<sub>3</sub> with trigonal P-3m1 symmetry, and the corresponding lattice parameters  $a = b = 9.002 \text{ \AA}$ . They are consistent with the reported values (Peng and Xie, 2020; Morimoto et al., 2022). In contrast, the structure is different from that of the sample prepared by spin coating in a glove box. It is a tetragonal crystal structure with the space group I4/mcm, as shown in Figure 5d (Walukiewicz et al., 2004). The XRD pattern shown in Figure 5d is a typical pattern of MASnI<sub>3</sub> perovskite. However, the diffraction pattern observed in the XRD analysis does not match the reported positions of the crystal phases in the literature due to oxidation of the perovskite material (Yuan et al., 2022; Whitfield et al., 2016; Yao et al., 2017). Hence, the material prepared by the ITC method in air in this work may be an oxygen-rich MASnI<sub>3</sub> perovskite crystal.

Figure 6a plots the current–voltage (I–V) characteristics of MASnI<sub>3</sub> perovskite metal-semiconductor-metal-type photodetectors prepared by the ITC method in air and biased

TABLE 1 Optoelectronic properties of ITC and spin-coated MASnI<sub>3</sub> photodetectors in this work.

Method	Photocurrent (A) @15 V	Selectivity (photocurrent/dark current) @15 V	Detectivity (Jones)	Photoresponsivity (A/W)
ITC	$4.83 \times 10^{-6}$	15.6	$2.82 \times 10^{13}$	49.56
spin-coating	$2.25 \times 10^{-4}$	608.1	$3.28 \times 10^{14}$	1926.24

TABLE 2 Comparison of the detectivity of the photodetectors as reported in the literature with our work.

Device Type	This Work	Nanosheets (Lan et al., 2017)	Crystal (Zhang et al., 2018)	Diode (Li et al., 2022)	Nanorods (Yao et al., 2024)
Detectivity (Jones)	$3.28 \times 10^{14}$	$3.1 \times 10^{11}$	$2.62 \times 10^{13}$	$5 \times 10^{12}$	$7.3 \times 10^{10}$

from 0 V to 15 V. The MASnI<sub>3</sub> perovskite photodetector exhibited smaller operating resistance under the light-off condition than in other situations without incident light. However, when the MASnI<sub>3</sub> perovskite photodetector was operated in light-on conditions, the conductivity of the MASnI<sub>3</sub> perovskite photodetector decreased. That means the defects in the MASnI<sub>3</sub> perovskite film were filled by photo-induced electrons, such that the migration ability of electrons decreases. For the device, the largest photocurrent ( $4.83 \times 10^{-6}$  A at 15 V) was observed when the wavelength of incident light was 700 nm. This is consistent with the band gap of the MASnI<sub>3</sub> material. Figure 6b plots the current–voltage (I–V) characteristics of MASnI<sub>3</sub> perovskite metal–semiconductor–metal type photodetectors prepared by the spin-coating method in a glove box and biased from 0 V to 15 V. For the device, the largest photocurrent ( $2.25 \times 10^{-4}$  A at 15 V) was observed when the wavelength of incident light was 700 nm. The photocurrent of a device prepared in a glove box is two orders of magnitude higher than that of the device prepared by the ITC method. It may contribute to the conductivity of the MASnI<sub>3</sub> perovskite film prepared by the spin-coating method in a glove box, which is better than that of the MASnI<sub>3</sub> perovskite film prepared by the ITC method in a glove box due to the almost moisture-free environment and ambient oxygen.

Figure 7 shows the photocurrent of MASnI<sub>3</sub> perovskite photodetectors prepared by the ITC and spin-coating methods at a bias of 15 V. Figure 8 plots the photoresponsivity of MASnI<sub>3</sub> perovskite metal–semiconductor–metal type photodetectors prepared by the ITC and spin-coating methods, respectively, at a bias of 15 V. The photoresponsivity and detectivity of the MASnI<sub>3</sub> perovskite photodetectors prepared by the ITC and spin-coating methods are 49.56 A/W and 1926.24 A/W under incident light of 650 nm, respectively, corresponding to  $2.82 \times 10^{13}$  and  $3.28 \times 10^{14}$  Jones. As shown in Figures 7, 8, the photocurrent obviously increases as the wavelength of incident light is in the range of 550–700 nm, then cuts off over 700 nm due to the absorption edge of the material. Therefore, the MASnI<sub>3</sub> perovskite can be used to apply the photodetector with a very narrow wavelength ranging from 550 to 700 nm. Table 1 lists the optoelectronic properties of ITC and spin-coated MASnI<sub>3</sub> photodetectors in this work. Although

the ITC-prepared film exhibits better crystallinity, it results in lower device performance than the spin-coated film. It may contribute to the defect states or charge transport limitations in perovskite oxide with high resistance, according to the I–V characteristics, as shown in Figure 6. In addition, Table 2 summarizes the comparison of the detectivity of the photodetector as reported in the literature with our work. This work demonstrates the best performance.

## 4 Conclusion

In summary, the characteristics of two kinds of MASnI<sub>3</sub> perovskite metal–semiconductor–metal-type photodetectors prepared by the ITC and spin-coating methods, respectively, have been demonstrated. The peaks of the photoluminescence (PL) spectrum of MASnI<sub>3</sub> perovskite films obtained by the inversion crystallization and the spin-coating methods are 470 nm, corresponding to 2.638 eV, and 750 nm, corresponding to 1.647 eV, respectively. A Burstein–Moss shift is observed due to the introduction of oxygen. In addition, the photocurrent of a device prepared in a glove box is two orders of magnitude higher than that of the device prepared by the ITC method. The MASnI<sub>3</sub> perovskite photodetector prepared by the ITC method in air exhibited higher operating resistance under the condition of illumination than that of the MASnI<sub>3</sub> perovskite photodetector prepared by the spin-coating method in a glove box. That means the MASnI<sub>3</sub> perovskite film has more defects induced by oxygen, such that the migration ability of the electrons decreases. The largest photocurrents of the MASnI<sub>3</sub> perovskite photodetector prepared by the ITC and spin-coating methods are  $4.83 \times 10^{-6}$  A and  $2.25 \times 10^{-4}$  A at 15 V, respectively. The photocurrent increases as the wavelength of incident light is in the range of 550–700 nm, then cuts off over 700 nm due to the absorption edge of the material. Therefore, the MASnI<sub>3</sub> perovskite can be used in the application of a photodetector with a very narrow wavelength, ranging from 600 to 700 nm. Finally, in this work, we found that the crystallinity of the sample prepared by the ITC method is better than that of the sample prepared by the spin-coating method. However, the performance of the sample prepared by the ITC method is inferior to that of the sample prepared by the

spin-coating method. In addition, we found that the sample is very easy to oxidize, but it will recover after being put back into the glove box. Hence, it can be used in an oxygen-free environment.

## Data availability statement

The original contributions presented in the study are included in the article/supplementary material; further inquiries can be directed to the corresponding author.

## Author contributions

W-SW: conceptualization, formal analysis, investigation, resources, and writing – review and editing. Y-CC: data curation, investigation, methodology, and writing – review and editing. T-YL: conceptualization, investigation, methodology, and writing – review and editing. L-CC: conceptualization, funding acquisition, project administration, writing – original draft, and writing – review and editing.

## Funding

The author(s) declare that financial support was received for the research and/or publication of this article. This research was funded

## References

- Aldamasy, M., Iqbal, Z., Li, G., Pascual, J., Alharthi, F., Abate, A., et al. (2021). Challenges in tin perovskite solar cells. *Phys. Chem. Chem. Phys.* 23, 23413–23427. doi:10.1039/d1cp02596a
- Bouich, A., Mari-Guaita, J., Soucase, B. M., and Palacios, P. (2022). Manufacture of high-Efficiency and stable lead-free solar cells through Antisolvent Quenching Engineering. *Nanomaterials* 12 (17), 2901. doi:10.3390/nano12172901
- Chen, L. C., Lan, W. H., Lin, R. M., Shen, H. T., and Chen, H. C. (2006). Optical properties of  $\text{In}_2\text{O}_3$  oxidized from InN deposited by reactive magnetron sputtering. *Appl. Sur. Sci.* 252, 8438–8441. doi:10.1016/j.apsusc.2005.11.051
- Chen, L. C., Tseng, Z. L., and Huang, S. K. (2016). A study of inverted-type perovskite solar cells with various composition ratios of  $(\text{FAPbI}_3)_{1-x}(\text{MAPbBr}_3)_x$ . *Nanomaterials* 6, 183. doi:10.3390/nano6100183
- Hao, F., Stoumpos, C. C., Cao, D. H., Chang, R. P. H., and Kanatzidis, M. G. (2014). Lead-free solid-state organic–inorganic halide perovskite solar cells. *Nat. Phot.* 8, 489–494. doi:10.1038/nphoton.2014.82
- Hao, F., Stoumpos, C. C., Guo, P., Zhou, N., Marks, T. J., Chang, R. P. H., et al. (2015). Solvent-mediated crystallization of  $\text{CH}_3\text{NH}_3\text{SnI}_3$  films for Heterojunction Depleted perovskite solar cells. *J. Am. Chem. Soc.* 137, 11445–11452. doi:10.1021/jacs.5b06658
- Kassa, E. E., Kurniawan, A., Wu, Y. F., and Biring, S. (2025). Achieving high response of perovskite-based  $(\text{MAPbI}_3)$   $\text{NH}_3$  gas sensors using binary mixed solvent approaches. *Sens. Actuators, A* 383, 116116. doi:10.1016/j.sna.2024.116116
- Lan, C., Dong, R., Zhou, Z., Shu, L., Li, D., Yip, S., et al. (2017). Large-scale synthesis of freestanding layer-structured  $\text{PbI}_2$  and  $\text{MAPbI}_3$  nanosheets for high-performance photodetection. *Adv. Mater.* 29, 1702759. doi:10.1002/adma.201702759
- Lee, C. C., Kurniawan, A., Iskandar, J., Chu, C. S., and Liu, C. Y. (2025). Achieving high response of perovskite-based  $(\text{MAPbI}_3)$  ammonia gas sensors at room temperature via light enhancement. *J. Mater. Chem. C* 13, 5140–5147. doi:10.1039/d4tc04522j
- Li, Z., Jiang, L., Rong, X., Dong, Q., Dong, H., Wang, L., et al. (2022).  $\text{MAPbI}_3$  photodetectors with 4.7 MHz bandwidth and their application in organic optocouplers. *J. Phys. Chem. Lett.* 13, 815–821. doi:10.1021/acs.jpclett.1c04137
- Mitzi, D. B., and Liang, K. (1997). Synthesis, resistivity, and thermal properties of the cubic perovskite  $\text{NH}_2\text{CH}=\text{NH}_2\text{SnI}_3$  and related systems. *J. Solid State Chem.* 134, 376–381. doi:10.1006/jssc.1997.7593
- Morimoto, M., Kawano, S., Miyamoto, S., Miyazaki, K., Hayase, S., and Iikubo, S. (2022). Electronic structure and thermal conductance of the  $\text{MASnI}_3/\text{Bi}_2\text{Te}_3$  interface: a first-principles study. *Sci. Rep.* 12, 217. doi:10.1038/s41598-021-04234-3
- Noel, N. K., Stranks, S. D., Abate, A., Wehrenfennig, C., Guarnera, S., Haghighirad, A. A., et al. (2014). Lead-free organic–inorganic tin halide perovskites for photovoltaic applications. *Energy Environ. Sci.* 7, 3061–3068. doi:10.1039/c4ee01076k
- Peng, L., and Xie, W. (2020). Theoretical and experimental investigations on the bulk photovoltaic effect in lead-free perovskites  $\text{MASnI}_3$  and  $\text{FASnI}_3$ . *RSC Adv.* 10, 14679–14688. doi:10.1039/d0ra02584d
- Sabba, D., Mulmudi, H. K., Prabhakar, R. R., Krishnamoorthy, T., Baikie, T., Boix, P. P., et al. (2015). Impact of anionic Br– substitution on open circuit voltage in lead free perovskite ( $\text{CsSn}_{1-x}\text{Br}_x$ ) solar cells. *J. Phys. Chem. C* 119, 1763–1767. doi:10.1021/jp512662a
- Saha, P., Singh, S., and Bhattacharya, S. (2024). Performance optimization of  $\text{MASnI}_3$  perovskite solar cells: insights into device architecture. *Micro Nanostructures* 191, 207827. doi:10.1016/j.micrna.2024.207827
- Stoumpos, C. C., Malliakas, S. D., and Kanatzidis, M. G. (2013). Semiconducting tin and lead iodide perovskites with organic cations: phase transitions, high mobilities, and near-infrared photoluminescent properties. *Inorg. Chem.* 52, 9019–9038. doi:10.1021/ic401215x
- Walukiewicz, W., Li, S. X., Wu, J., Yu, K. M., Ager III, J. W., Haller, E. E., et al. (2004). Optical properties and electronic structure of InN and In-rich group III-nitride alloys. *J. Cryst. Growth* 269, 119–127. doi:10.1016/j.jcrysgro.2004.05.041
- Wan, J., Yu, X., Zou, J., Li, K., Chen, L., Peng, Y., et al. (2021). Lead contamination analysis of perovskite modules under simulated working conditions. *Sol. Energy* 226, 85–91. doi:10.1016/j.solener.2021.08.031
- Whitfield, P. S., Herron, N., Guise, W. E., Page, K., Cheng, Y. Q., Milas, I., et al. (2016). Structures, phase transitions and tricritical behavior of the hybrid perovskite methyl ammonium lead iodide. *Sci. Rep.* 6, 35685. doi:10.1038/srep35685
- Yao, Z., Xiong, Y., Kang, H., Xu, X., Guo, J., Li, W., et al. (2024). Tunable periodic nanopillar array for  $\text{MAPbI}_3$  perovskite photodetectors with improved light absorption. *ACS Omega* 9, 2606–2614. doi:10.1021/acsomega.3c07390

by the National Science and Technology Council of Taiwan, grant number 111-2221-E-027-040-MY3.

## Conflict of interest

The authors declare that the research was conducted in the absence of any commercial or financial relationships that could be construed as a potential conflict of interest.

## Generative AI statement

The authors declare that no Generative AI was used in the creation of this manuscript.

## Publisher's note

All claims expressed in this article are solely those of the authors and do not necessarily represent those of their affiliated organizations, or those of the publisher, the editors and the reviewers. Any product that may be evaluated in this article, or claim that may be made by its manufacturer, is not guaranteed or endorsed by the publisher.

Yao, Z., Yang, Z., Liu, Y., Zhao, W., Zhang, X., Liu, B., et al. (2017). Local temperature reduction induced crystallization of  $\text{MASnI}_3$  and achieving a direct wafer production. *RSC Adv.* 7, 38155–38159. doi:10.1039/c7ra07101a

Yuan, Z., Zhou, J., Zhang, Y., Ma, X., Wang, J., Dong, J., et al. (2022). Growing  $\text{MASnI}_3$  perovskite single-crystal films by inverse temperature crystallization. *J. Phys. Cond. Matter* 34, 144009. doi:10.1088/1361-648x/ac4c64

Zhai, Y., Duan, G., Hu, J., Ly, Z., Ding, G., Zhou, Y., et al. (2024). Device-level in-sensor olfactory perception system based on array of  $\text{PCBM-MAPbI}_3$  heterostructure transistors. *Adv. Funct. Mater.* 34, 2406239. doi:10.1002/adfm.202406239

Zhang, Y., Liu, Y., Yang, Z., and Liu, S. (2018). High-quality perovskite  $\text{MAPbI}_3$  single crystals for broad-spectrum and rapid response integrate photodetector. *J. Energy Chem.* 27, 722–727. doi:10.1016/j.jechem.2017.11.002